Available online at www.sciencedirect.com
SCIENCE DIRECT®
ELSEVIER
Earth and Planetary Science Letters 216 (2003) 1–15
EPSL
www.elsevier.com/locate/epsl

The mechanism of great Banda Sea earthquake of 1 February 1938: applying the method of preliminary determination of focal mechanism to a historical event

Emile A. Okal [a,*], Dominique Reymond [b]

[a] *Department of Geological Sciences, Northwestern University, Evanston, IL 60201, USA*
[b] *Laboratoire de Détection et Géophysique, Commissariat à l'Energie Atomique, P.O. Box 640, F-98713 Papeete, Tahiti, French Polynesia*

Received 20 May 2003; received in revised form 15 August 2003; accepted 21 August 2003

Abstract

A moment tensor solution is derived for the great 1938 Banda Sea earthquake, one of the largest events for which no definitive focal geometry has been published. We apply the method of preliminary determination of focal mechanism, which consists of inverting for a moment tensor using exclusively the spectral amplitudes of mantle Rayleigh and Love waves, while discarding the phase information which can be affected by uncertainties in relative timing between historical records. From a dataset of 17 records at seven stations, we obtain a robust solution, featuring a very large moment of 8.37×10^{28} dyn-cm, the centroid depth being constrained around 60 km by minimizing the rms residual of the inversion. The method involves an inherent two-fold 180° indeterminacy on the orientations of strike and slip, which is lifted by the examination of the polarization of long-period body waves read individually on original records, resulting in a mostly thrust-faulting mechanism (strike: 276°; dip: 63°; slip: 70°). This approach, coupled with more traditional relocation efforts, allows a rare glimpse of this exceptional event, confirmed here to rank among the 10 largest moments ever published. Within the extremely complex regional plate tectonics pattern, the 1938 event took place in a region of sparse seismicity, and away from the presumed locations of block boundaries. The deeper than normal focus of the event agrees well with the generally minor level of reported damage, and with the generation of a relatively benign tsunami. Available modern focal mechanisms in its vicinity are too few and too scattered to allow any meaningful comparison, but the 1938 event shares its compressional axis with that of the smaller and deeper 1963 shock to the southwest, which probably expresses coherence in the regional contortion of the subducting Australian plate lithosphere.

Keywords: moment tensor inversions; historical earthquakes; Banda Sea; Indonesia

1. Introduction

The purpose of the present study is to test a variation of seismic moment tensor inversion introduced in a previous contribution ([1]; hereafter

* Corresponding author. Tel.: +1-847-491-3194; Fax: +1-847-491-8060.
E-mail address: emile@earth.nwu.edu (E.A. Okal).

0012-821X/03/$ – see front matter © 2003 Elsevier B.V. All rights reserved.
doi:10.1016/S0012-821X(03)00475-8

Paper I) on one of the largest historical earthquakes for which no definitive focal mechanism has been published, namely the Banda Sea event of 1 February 1938. This earthquake was given a Pasadena magnitude of 8.6 by Gutenberg and Richter [2], and its moment was estimated at 7×10^{28} dyn-cm by Kanamori [3], based on the 100-s spectral amplitudes reported by Brune and Engen [4]. Okal [5] measured mantle magnitudes M_m between 8.75 and 9.04 ($M_0 = 5.6\times10^{28}$–1.1×10^{29} dyn-cm) from long-period records at the three stations PAS, COL, and UPP; his study forms the embryo of the present work.

In Paper I, we presented the method of preliminary determination of focal mechanisms (PDFM) based on the inversion of mantle wave spectral amplitudes. Following an idea originally proposed by Romanowicz and Suárez [6], we showed that the inversion of depleted datasets of spectral amplitudes could lead to robust moment tensor solutions from as few as three stations. We were motivated by the fact that the correct interpretation of spectral phases requires knowledge of the phase velocity along the path with an accuracy of 0.5% [7], which may not be available in real time under operational conditions, notably in the context of tsunami warning. This limitation of a standard centroid moment tensor (CMT) inversion can be alleviated by discarding the phase information and inverting only spectral amplitudes – at the cost of a double 180° indeterminacy on the strike and slip angles of the final solution. As discussed in [6], the moduli of surface wave spectra remain unchanged both when flipping the slip angle 180°, which merely reverses the sense of faulting and hence multiplies all spectra by -1, and when rotating the azimuth of fault strike by 180°, which changes all complex spectra excited at the source into their complex conjugates.

A similar situation arises in the study of historical earthquakes, for which precise timing corrections for original seismograms are often lost, thus precluding the use of relative phase information between stations. For example, Huang et al. [8] were restricted to one-station datasets in their moment tensor inversions of pre-1962 deep earthquakes. Their technique fails, however, for shallow events, as they feature inadequate overtone excitation.

In the case of the 1938 Banda Sea earthquake, we show that a robust inversion is possible from a dataset of 17 mantle waves recorded at seven stations. The ambiguity in focal mechanism is then lifted by considering polarizations of P and S waves at critical stations. Our results confirm the 1938 event as one of the 10 largest earthquakes in terms of measured M_0.

1.1. Tectonic background

The 1938 Banda Sea earthquake took place in one of the most complex tectonic regions on Earth, in the general framework of the double collision of continental Australia and the oceanic Pacific and Philippine plates with the southernmost tip of the Eurasian plate, called 'Sundaland'. As a result, the region is composed of a large number of geological provinces, described in detail by Hamilton [9], whose relative motions have been inferred recently from GPS measurements (e.g., [10,11]). In particular, the eastern termination of the Banda Sea features a number of strongly curved, concentric tectonic provinces. Proceeding westwards (inwards) from the Arafura Sea (Fig. 1), these are:

1. the Aru Islands, composed of originally uplifted carbonates, presently undergoing subsidence in the context of the development of subduction at the Aru Trough [12];
2. the Aru Trough, representing the modern position of the boundary of the Australian plate, and featuring a 3500-m-deep trench, which expresses the continuation of the outer Java and Timor Trough to the east;
3. the Kai and Tanimbar Island groups, which prolong the outer island arc (Timor, Leti, Babar), and consist of much deformed mélanges of shallow-water limestones, marl, and various clastic sedimentary and crystalline rocks, as summarized by Hamilton [9] and Charlton et al. [13]. To the north of the Kai Islands, the arc bends west into the small Tajandu and Watubela islands, before linking up with Seram;
4. the deep Weber Basin, reaching 7500 m, whose

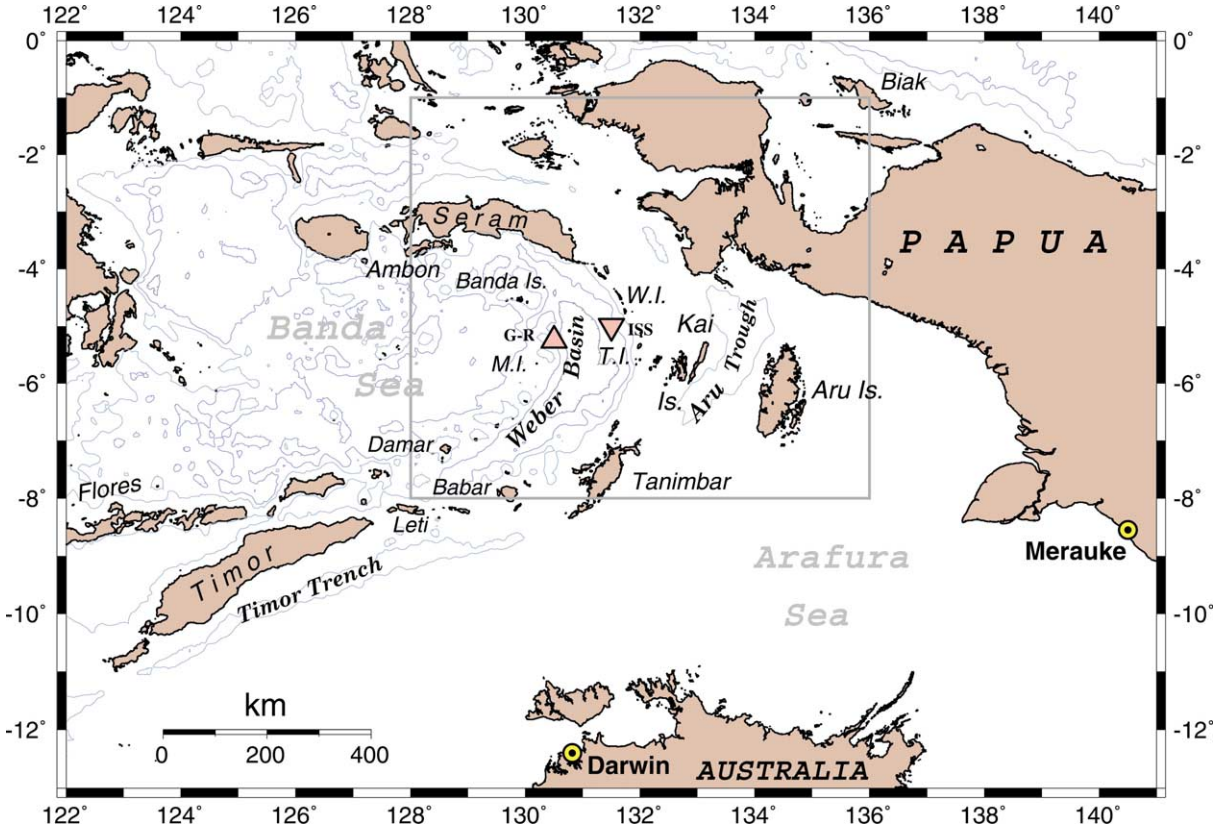

Fig. 1. Location map of the area under study. Bathymetric contours are at 2000-m intervals. T.I.: Tajandu Island group; W.I.: Watubela Island group; M.I.: Manuk Island. The downward-pointing triangle is the epicenter of the 1938 event from the ISS, the upward-pointing triangle that proposed by Gutenberg and Richter [5]. The gray box outlines the boundaries of the map in Fig. 2.

tectonic interpretation remains unclear [14], with McCaffrey [15] proposing that it simply expresses the uncompensated motion of the sinking lithosphere subducting at the Aru Basin to the east;

5. An arc of small islands, extending from Damar to Manuk, expressing the continuation of the volcanically active inner arc comprising Bali, Sumbawa, and Flores. Note however that active volcanism may be displaced $\sim$130 km to the north at the longitude of Timor ([9], pp. 118 and 149).

The distribution of seismicity in the region is itself very complex, and has been the subject of many studies (e.g., [16–19]), but a definitive interpretation is still controversial [15,20]. Fig. 2 shows background seismicity in our study area, as relocated by Engdahl et al. ([21], and personal communication) for the period 1963–1999. In general, the whole Sunda–Banda arc lacks mega-thrust interplate earthquakes: as noted by Hamilton [9], subduction at the Java and Timor troughs is largely aseismic; the only large shallow thrust event ($M_0 \geq 10^{27}$ dyn-cm) in the Harvard CMT catalog ([22] and subsequent quarterly updates) is the 1992 Flores earthquake, located to the north of the volcanic inner arc, and expressing southward subduction of the Flores Sea under the inner arc. Further east, and in our study area, we note that the Aru Islands are essentially aseismic (e.g., [17]), while the Aru Basin does feature shallow seismicity ($h \leq 50$ km) north of 6°S. This prompted McCaffrey [15] to identify the basin as the locus of active oblique subduction of

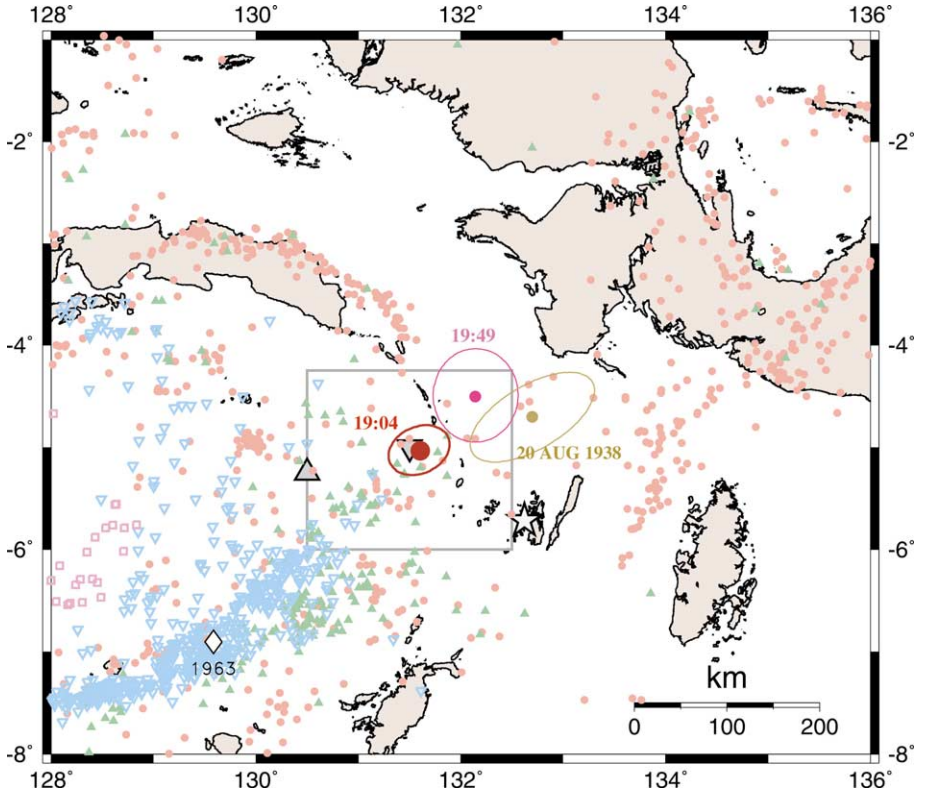

Fig. 2. Relocation of the 1938 event and its aftershocks. The small symbols show the background seismicity from Engdahl et al.'s [21] catalog, coded by depth: solid dots $h < 50$ km; solid triangles, $50 \leq h < 100$ km, open inverted triangles $100 \leq h < 300$ km, open squares $h \geq 300$ km. The large solid dot is our relocated epicenter for the main shock at 19:04 GMT (with fat Monte Carlo ellipse), the smaller symbols and thinner ellipses show the relocations of the two aftershocks (see text for details and Fig. 1 for geographic names). The diamond shows the epicenter of the 1963 Banda Sea intermediate-depth earthquake [42] and the star the location of the reported emergence of a new island [25]. The gray box outlines the boundaries of the map in Fig. 3.

the Australian Plate. Note however that no interplate thrusting earthquakes are documented in the basin, with the only substantial CMT solutions ($M_0 > 10^{25}$ dyn-cm) expressing normal faulting. This probably reflects the strong obliquity of the subduction. Proceeding west, seismicity is very sparse in the Kai group where the few available CMT solutions feature a strike-slip geometry. In the Weber Basin, deeper hypocenters are present, interpreted by McCaffrey [15] as expressing both northward subduction under the Timor–Tanimbar arc in the south, and southward subduction under Seram and the Ambon arc [23] to the north. Their focal mechanisms are broadly scattered, even on a regional scale.

In this general framework, the epicenter of the 1938 event was given by Gutenberg and Richter [2] as 5.25°S, 130.5°E, under the small island of Manuk (Fig. 1), part of the volcanically active inner arc, and by the International Seismological Summary (ISS) at 5.0°S, 131.5°E, i.e., at the eastern boundary of the Weber deep, west of the Tajandu–Watubela Island group.

2. Relocation

We relocated the 1938 Banda Sea event using the interactive iterative technique of Wysession et al. [24], based on a dataset of 73 P arrivals reported by the ISS. This dataset has essentially no depth resolution: floating-depth relocations fail to converge, and epicenters move only 7 km when depth is constrained between 0 and 100 km,

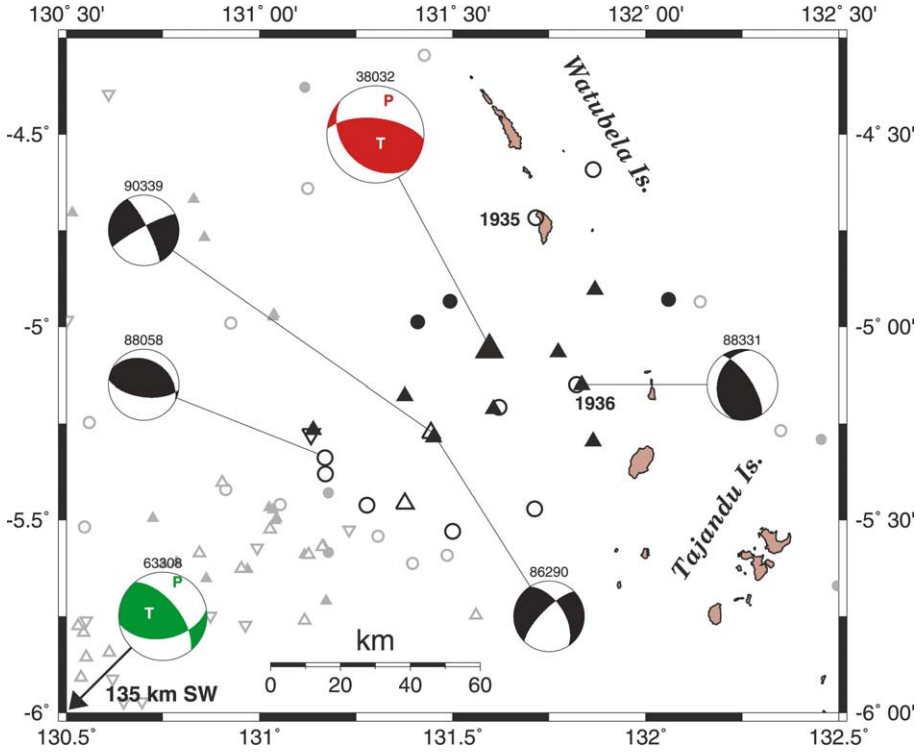

Fig. 3. Close-up of the epicentral area of the 1938 earthquake. The 23 events identified as located within 60 km of the epicenter are shown as the large dark symbols, and coded by depth: solid dots, $h < 30$ km; open circles, $30 \leq h < 50$ km; solid triangles, $50 \leq h < 75$ km; open triangles, $75 \leq h < 100$ km; and inverted open triangle, $h > 100$ km. Note that they do not define a simple slab. Similarly coded are the more distant events from Fig. 2, shown as smaller, gray symbols. Focal mechanisms, identified by Julian dates, are shown for the four available Harvard CMT solutions (note scatter in focal geometry), the solution inverted in the present study (38032), and the 1963 earthquake (63308), as obtained by Welc and Lay [46]. The latter event is shown for reference, since it plots outside the map.

with rms residuals increasing only from 3.7 to 3.9 s. In anticipation of our results in Section 3, we use a constrained depth of 60 km, and obtain our preferred solution at 5.06°S, 131.60°E, origin time 19:04:22.9 GMT ($\sigma = 3.74$ s). This solution is remarkably stable with respect to the choice of the trial epicenter required by the relocation algorithm, even when the latter is selected in the Atlantic Ocean, at the antipodes of the final solution. It is also essentially identical to the epicenter (5.059°S, 131.62°E) obtained using Engdahl et al.'s [21] algorithm (E.R. Engdahl, personal communication, 2002). The injection of Gaussian noise with $\sigma_G = 5$ s (a value appropriate for the 1930s) results in a well contained Monte Carlo ellipse of only 32 km in semi-major axis (Fig. 2). In summary, the earthquake relocates essentially at the ISS epicenter, but about 120 km east of Gutenberg and Richter's [2] location; this in itself constitutes a rather unusual occurrence in the study of historical earthquakes.

One large aftershock is documented 45 min after the main shock, and only one more event (on 20 August 1938) is listed in the area by the ISS for the whole year following the main shock. However, many small aftershocks were reported locally in the days following the main shock [25]. The same-day aftershock relocates at 4.54°S, 132.13°E, 82 km northeast of the main shock. A floating-depth relocation converges on 39 km, but the dataset has no depth resolution under Wysession et al.'s [24] Monte Carlo algorithm, run with $\sigma_G = 5$ s. The August aftershock relocates at 4.74°S, 132.67°E, 123 km east-northeast of the

main shock, with no control on depth. Fig. 2 summarizes the relative location of the main shock and its two aftershocks.

2.1. Background seismicity in the vicinity of the epicenter

In order to place the relocated 1938 hypocenter in the context of background seismicity, we consider separately pre- and post-1963 events. For the latter, we use Engdahl et al.'s [21] catalog of relocated hypocenters, from which we extract 21 earthquakes whose epicenter is less than 60 km away from our relocation. For historical events, we extracted from the NEIC dataset those events after 1940 with an epicenter less than 100 km away from the relocated 1938 epicenter, and increased the threshold to 150 km between 1910 and 1940. In addition to the 1938 main shock and its two aftershocks, we found 24 events, which we relocated systematically, using Wysession et al.'s [24] algorithm. Only two shocks relocate less than 60 km from the 1938 earthquake: the event of 31 October 1935, 40 km to the north-northeast with a source depth of 48 km, and that of 4 November 1936, only 29 km to the east-southeast with a source depth of 70 km. Both Monte Carlo ellipses for these events intersect that of the 1938 shock, but neither of their depths can be constrained under the Monte Carlo algorithm.

The resulting 23 neighbors to the 1938 epicenter (excluding the two aftershocks discussed above) are plotted in Fig. 3. These events are generally small (maximum magnitude $m_b = 6.2$ for the modern ones; no magnitude available for the two historical shocks). Their depths range from 18 to 109 km (most of them clustered between 40 and 75 km), but they do not define a clear planar or even curving slab. The closest events to the 1938 epicenter are 17 km away.

In conclusion, the 1938 Banda Sea earthquake took place under the outer island arc, slightly west of the gap between the Tajandu and Watubela groups, at the extreme eastern boundary of the Weber Basin, as opposed to under the volcanic arc, as suggested by Gutenberg and Richter [2]. Within the Banda Sea, a region of generally high seismic activity (see Fig. 2), the immediate epicentral region has documented, but relatively low, seismicity with only 23 earthquakes since 1910 known to relocate less than 60 km from the 1938 epicenter (Fig. 3). By contrast, a modern event at comparable depth in a well-developed Benioff zone, such as the Central Chilean slab,

Table 1
Seismological dataset used in the PDFM inversion

Station				Wavetrain	Distance	Azimuth	Importance
Code	Location	Instrument	Component		(°)	(°)	I
ABU	Abuyama, Japan	Wiechert	EW	G_1	39.99	5.10	0.654
COL	College, Alaska	McRomberg	EW	R_1	90.60	24.90	1.334
COL	College, Alaska	McRomberg	NS	G_1	90.60	24.90	0.031
HON	Honolulu, Hawaii	Milne-Shaw	NS	G_1	73.76	66.22	0.218
PAS	Pasadena, California	Benioff 1–100	EW	R_1	109.55	55.71	0.597
PAS	Pasadena, California	70-s Torsion	NS	G_1	109.55	55.71	0.096
PAS	Pasadena, California	70-s Torsion	NS	G_2	250.45	235.71	0.096
PAS	Pasadena, California	70-s Torsion	NS	G_3	469.55	55.71	0.096
PAS	Pasadena, California	70-s Torsion	NS	G_4	610.45	235.71	0.096
SJG	San Juan, Puerto Rico	Wenner	NE–SW	G_1	158.32	51.91	0.103
SJG	San Juan, Puerto Rico	Wenner	NE–SW	G_3	518.32	51.91	0.103
SJG	San Juan, Puerto Rico	Wenner	NE–SW	G_4	561.68	231.91	0.103
UPP	Uppsala, Sweden	Wiechert	NS	R_1	106.25	331.27	1.059
UPP	Uppsala, Sweden	Wiechert	EW	G_1	106.25	331.27	0.125
UPP	Uppsala, Sweden	Wiechert	EW	G_2	253.75	151.27	0.125
UPP	Uppsala, Sweden	Wiechert	EW	G_3	466.25	331.27	0.125
WES	Weston, Massachusetts	Benioff 1–60	EW	G_3	497.55	25.38	0.038

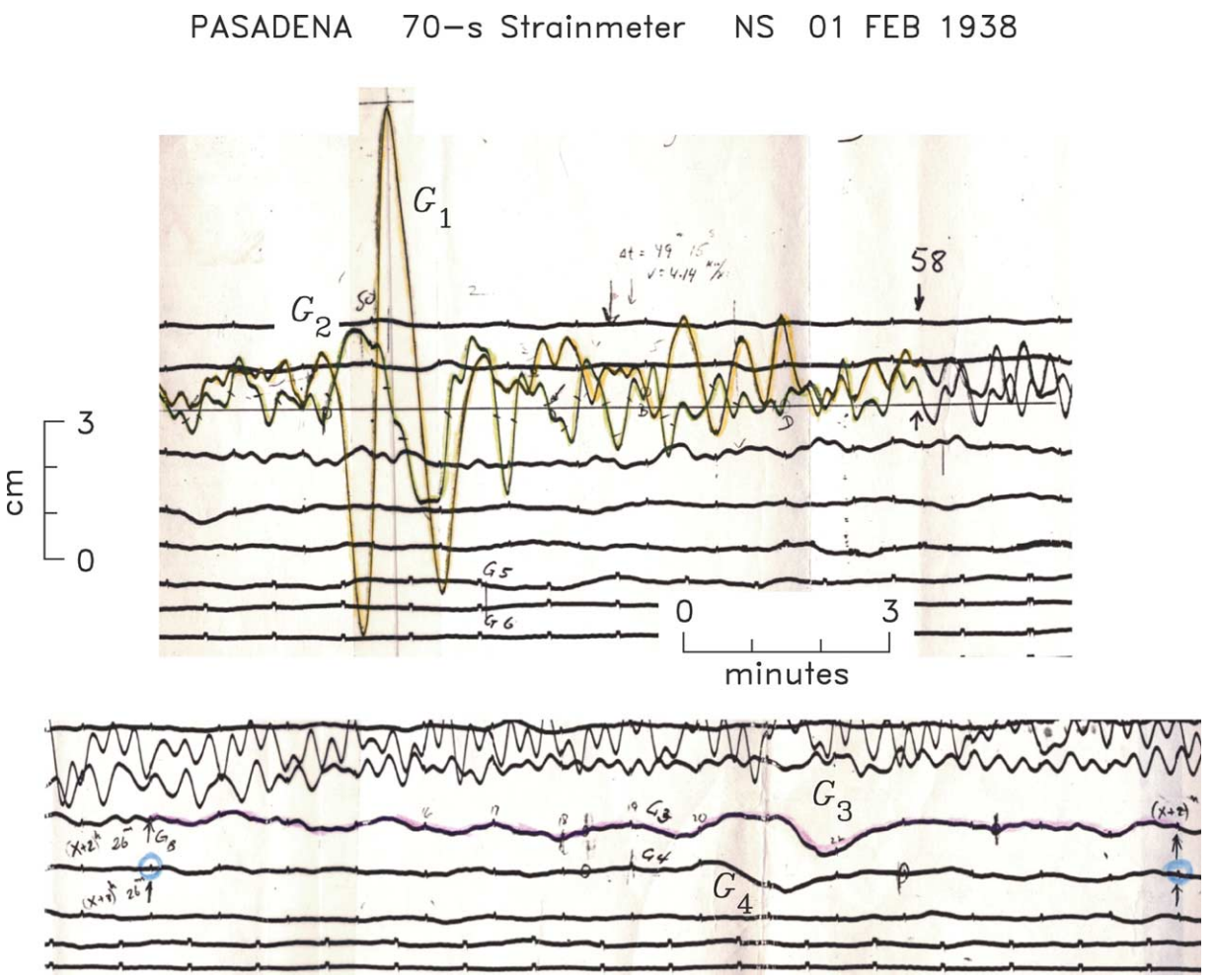

Fig. 4. Original NS strainmeter record at Pasadena, showing the G_1 and G_2 (top) and G_3 and G_4 (bottom) waveforms. The back-azimuth (277°) provides nearly pure transverse polarization.

would typically have more than 100 such neighbors in Engdahl et al.'s [21] dataset. The epicenter of the 1938 event is at least 250 km from the Aru Trough, interpreted as the boundary of the Australian plate [15,26]; this rules out an interplate character for this reportedly very large earthquake.

3. PDFM inversion

3.1. Dataset and methodology

Table 1 gives a list of the 17 waveforms used in the present study. In addition to the dataset used by Okal [5], we gathered records from a variety of sources, and digitized them to a common sampling rate of $\delta t = 1$ s. Fig. 4 shows relevant windows of the original strainmeter record at Pasadena. Information on instrument response, a critical parameter of any quantitative study of historical seismograms, was obtained from station log books or reconstructed from the catalogs of McComb and West [27] and Charlier and Van Gils [28]. Each record was processed through the TREMORS algorithm [29], to retrieve the spectral amplitude of ground displacement for each waveform in the window 90–300 s. The dis-

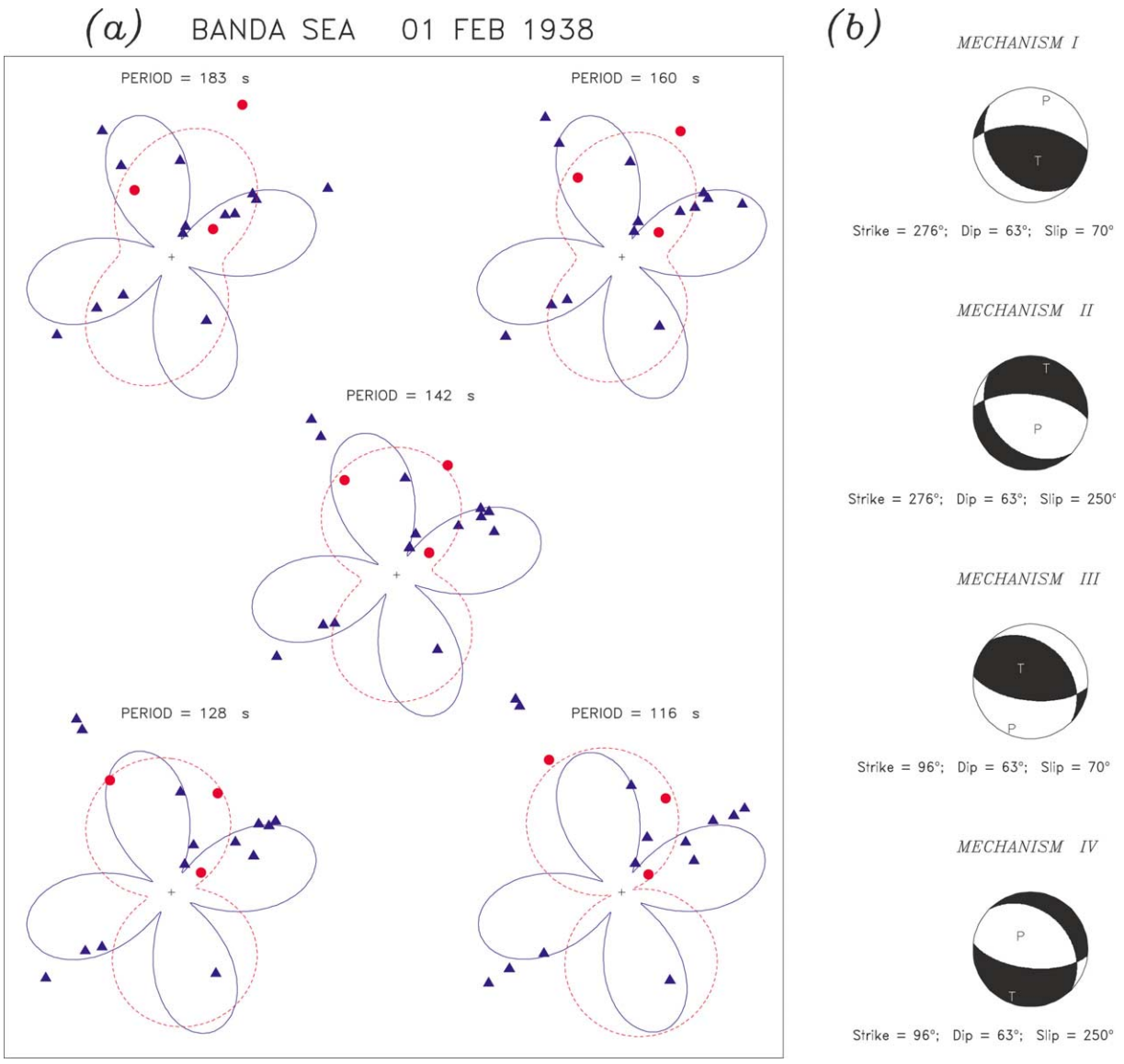

Fig. 5. (a) Radiation patterns of mantle waves for a number of representative periods. In each diagram, the individual symbols represent observed spectral amplitudes, and the continuous lines are the theoretical radiation patterns as a function of azimuth for the preferred inverted mechanism. Solid lines and triangles relate to Love waves, dashed lines and dots to Rayleigh waves. Scaling is common to Love and Rayleigh waves for each period, but varies between periods. (b) Lower-focal hemisphere representation of the major double couple of the preferred solution for all four geometries resulting from the double indeterminacy inherent in the PDFM method.

tance correction C_D defined by Okal and Talandier [30,31] was applied to eliminate the effect of both geometrical spreading and anelastic attenuation, but the source correction C_S was not applied.

For each record, the spectral amplitudes were then smoothed by a cubic spline as a function of frequency. In the notation of Paper I's equation 3, the resulting dataset consists of spectral amplitudes R_{ij} (for Rayleigh waves) and L_{ij} (for Love

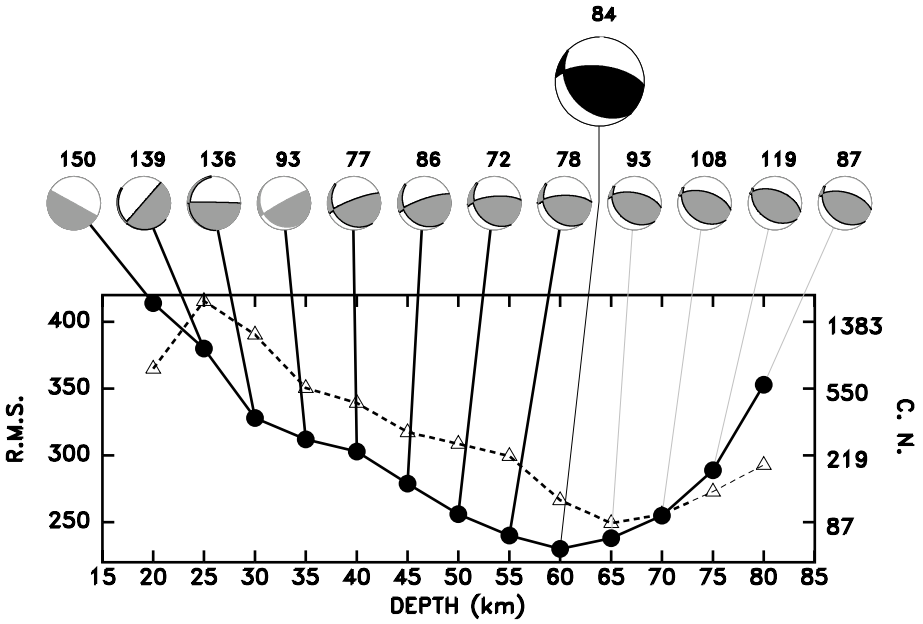

Fig. 6. Evolution of the inverted mechanism and of the quality of the inversion as a function of centroid depth. The solid line and the individual dots show the rms residual (in arbitrary units; left scale). The triangles and the dashed line show the condition number of the inversion (logarithmic scale at right). The inverted solutions are shown in gray (with scalar moment in units of 10^{27} dyn-cm), with the preferred solution highlighted by a larger, black beach ball.

waves) from 17 records (indexed j) at 10 equidistant frequencies (indexed i), in the period range 91–256 s. We then invert this dataset for the moment tensor components M_{kl} (under the deviatoric constraint $M_{kk}=0$), following the stepwise procedure detailed in Paper I. We restrict the frequency band to between 5 and 10 mHz: at lower frequencies, the response of some of the older instruments is insufficient, while for $f>10$ mHz, source finiteness effects and the presence of Love wave overtones [31] affect the inversion. A minimal amount of damping (1%) is used to protect the inversion from occasional instability without affecting its results. We also verified that our results were essentially unaffected by the introduction of a finiteness factor, as described in Paper I. Finally, Table 1 lists the individual importance, I, of each record in the formalism of Minster et al. [32]. In simple terms, these quantities express the number of degrees of freedom in the model controlled by each record; their sum should be 5, the dimension of parameter space.

3.2. Results

Our best solution for the moment tensor, obtained at a depth of 60 km, is $M_{rr}=69.6$, $M_{\theta\theta}=-50.0$, $M_{\phi\phi}=19.5$, $M_{r\theta}=-50.1$, $M_{r\phi}=-15.5$, $M_{\theta\phi}=25.0$, all components given in units of 10^{27} dyn-cm. The fit of the spectral amplitudes to the theoretical radiation patterns is shown in Fig. 5a. As explained in Paper I, ignoring the phase information in the waveforms results in a double indeterminacy, on the signs of all the M_{ij} components (which amounts to taking a mechanism with exact opposite polarity), or on the signs of the components $M_{r\theta}$ and $M_{r\phi}$ only (which amounts to rotating the mechanism 180° in azimuth, thus changing all spectral components into their complex conjugates).

This moment tensor can be decomposed into its major and minor double couples. The major double couple is shown in Fig. 5b (with all four geometries permitted by the double indeterminacy), and has a moment $M_0=8.37\times10^{28}$ dyn-

Table 2
Depth resolution and robustness of inversion

Description	Constrained depth	Scalar moment M_0	Focal mechanism			Deviation from preferred solution	
	(km)	(10^{27} dyn-cm)	ϕ (°)	δ (°)	λ (°)	r	Ω (°)
Preferred solution	60	83.66	276	63	70		
Depth varied							
Depth fixed at 20 km	20	150.2	299	90	90	0.25	37.4
Depth fixed at 25 km	25	138.6	221	90	85	0.22	65.8
Depth fixed at 30 km	30	136.3	271	89	80	0.21	28.5
Depth fixed at 35 km	35	92.94	241	85	74	0.046	42.7
Depth fixed at 40 km	40	76.87	249	81	69	−0.037	32.1
Depth fixed at 45 km	45	85.54	251	79	68	0.0097	29.6
Depth fixed at 50 km	50	72.07	265	71	65	−0.065	12.9
Depth fixed at 55 km	55	78.17	269	68	67	−0.030	8.7
Depth fixed at 65 km	65	92.69	281	60	74	0.045	5.0
Depth fixed at 70 km	70	108.2	286	57	78	0.112	11.1
Depth fixed at 75 km	75	119.2	290	53	81	0.154	15.8
Depth fixed at 80 km	80	87.30	285	59	76	0.019	8.5
Epicenter moved							
Moved east 5°	60	83.92	276	63	73	0.0014	6.5
Moved west 5°	60	84.82	274	63	70	0.0060	2.0
Moved north 5°	60	84.41	273	63	71	0.0039	3.8
Moved south 5°	60	86.18	273	63	76	0.013	8.4
Instrument gains reduced by 25%							
ABU	60	82.94	277	64	68	−0.0038	2.7
COL	60	99.16	282	61	76	0.074	5.6
HON	60	83.26	276	64	69	−0.0021	0.8
PAS Benioff	60	85.36	276	63	71	0.0087	1.9
PAS Strain	60	85.36	272	64	70	0.0087	4.3
SJG	60	84.52	274	63	71	0.0044	3.0
UPP	60	88.03	270	67	66	0.022	6.6
WES	60	83.61	276	63	70	−0.0003	0.0
Jack-knifing waveforms							
ABU G_1 suppressed	60	83.23	276	64	69	−0.0023	1.6
COL R_1 suppressed	60	61.21	258	86	62	−0.14	29.0
COL G_1 suppressed	60	83.57	276	63	71	−0.0005	1.5
HON G_1 suppressed	60	83.34	276	64	69	−0.0017	1.4
PAS R_1 suppressed	60	97.08	281	58	74	0.065	6.0
PAS G_1 suppressed	60	84.13	275	64	70	0.0024	2.3
PAS G_2 suppressed	60	84.24	276	63	71	−0.0022	1.0
PAS G_3 suppressed	60	83.60	276	63	71	−0.0003	1.0
PAS G_4 suppressed	60	83.79	275	63	71	0.0006	1.9
SJG G_1 suppressed	60	83.59	276	63	71	−0.0004	1.0
SJG G_3 suppressed	60	84.02	275	63	71	0.0019	1.9
SJG G_4 suppressed	60	83.98	275	63	71	0.0017	1.9
UPP R_1 suppressed	60	83.93	281	61	74	0.0014	5.2
UPP G_1 suppressed	60	84.12	275	63	71	0.0024	1.9
UPP G_2 suppressed	60	83.08	277	63	70	−0.0030	1.0
UPP G_3 suppressed	60	84.03	275	63	71	0.0019	1.9
WES G_3 suppressed	60	83.60	276	63	71	−0.0003	1.0

cm. The minor double couple amounts to 10.8% of M_0.

3.3. Depth

Centroid depth was resolved by minimizing the rms residual of the inversion at constrained depths ranging from 20 to 80 km. As shown in Fig. 6, a clear minimum is obtained at 60 km; we refer to this solution as 'preferred'. Following Paper I, we characterize the deviation of an inversion from our preferred solution through the logarithmic residual of the scalar moment, $r = \log_{10}(M_0^{\text{inverted}}/M_0^{\text{preferred}})$ and the 'Kagan angle', Ω, quantifying the smallest solid rotation separating the two beach ball representations of the moment tensors in three-dimensional space [33]. Table 2 and Fig. 6 show that, between 50 and 70 km, the inverted solution is essentially unchanged with Kagan angles less than 1° and absolute residuals smaller than 0.1 logarithmic unit. However, for shallower sources, the moment grows to much larger values, as the solution develops the classical $M_{r\theta}$, $M_{r\phi}$ singularity. For deeper sources, both geometry and moment deviate significantly while the quality of the fit deteriorates. We retain $h = 60$ km, which also comes close to minimizing the condition number C of the inversion, as defined in Paper I.

3.4. Robustness

Given the uncertainties involved in the study of historical earthquakes, we investigated the robustness of the inversion with respect to a number of potentially poorly constrained parameters. In the next sections, we vary those parameters systematically and examine the departure of the resulting inverted best double couple, with respect to the preferred solution, by means of the quantities r and Ω, which we list in Table 2, under a format mirroring that of table 1 in Paper I. We conclude that the inversion is indeed very robust.

3.4.1. Epicentral location

We start by artificially moving the epicenter 5° in all four directions. In practice, this amounts to covering most of the eastern Banda Sea, over distances far in excess of the epicentral uncertainty inferred from the relocation in Section 2. As shown in Table 2, the solution is essentially unchanged.

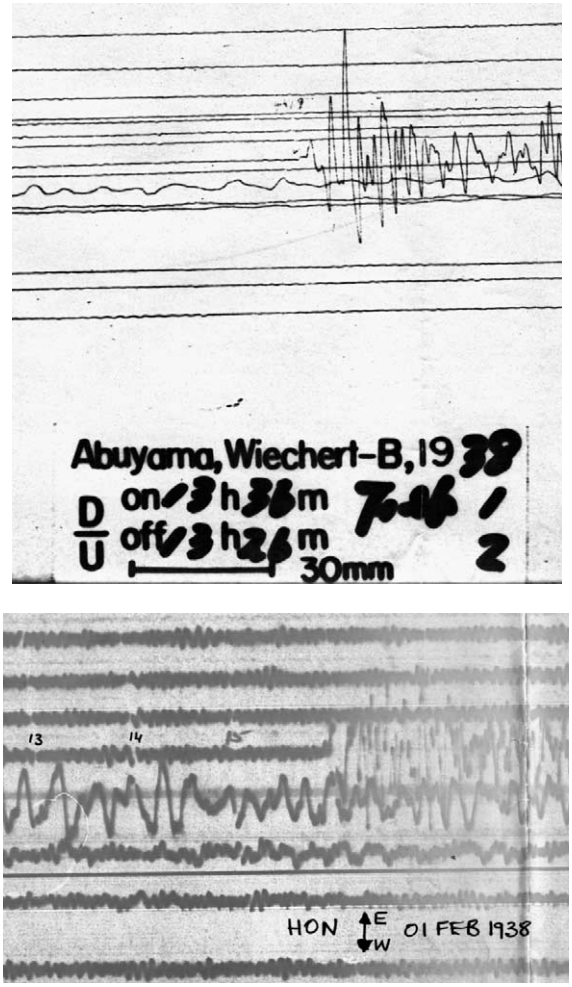

Fig. 7. Examples of body-wave polarizations allowing resolution of the four-fold indeterminacy of the focal mechanism. (Top) Vertical Wiechert record of the dilatational first arrival at Abuyama; the original label is reproduced, including record orientation (D-U). The time bar (30 mm) corresponds to 1 min. (Bottom) Milne–Shaw east–west record at Honolulu (back-azimuth 258°). Note P-wave first motion to east, i.e., away from the source. Numbers refer to minute marks after 19:00 GMT.

3.4.2. Instrument responses

In order to guard against possible uncertainties in instrument gains, and in particular in the opti-

cal magnifications involved at various stages of the data retrieval (usually asserted from the reconstruction of paper speed from minute marks), we then run a series of tests in which we artificially increase the spectral amplitude by 25% for each seismogram, one at a time. When several phases (e.g., G_1, G_2, G_3 at UPP) were recorded on the same seismogram, we apply the correction to all of them. Table 2 shows that the results are remarkably robust with Kagan angles of no more than a few degrees, and residuals r always less than 0.1 logarithmic unit (i.e., a factor of only 12% on M_0).

3.4.3. Jack-knifing

Finally, we further investigate the robustness of the inversion by so-called jack-knifing, i.e., running the inversion on datasets from which a single waveform is removed, one at a time. Table 2 includes the results of all possible 17 cases. Not surprisingly, removing those records with the largest values of the importance I (listed in Table 1) results in the largest deviations in the moment tensors. In this respect, the Rayleigh records are most crucial to the inversion, since they are the only ones resolving the component M_{rr}. Once again, the jack-knifed results are found to be remarkably robust.

3.5. Resolving the four-fold indeterminacy

In order to resolve the indeterminacy between the four possible mechanisms shown in Fig. 5b, we consider body-wave polarization constraints read directly on archived long-period seismograms. We were able to identify: (a) a downward P-wave polarization at ABU; (b) an eastward (anaseismic) polarization of P at HON (both shown in Fig. 7); (c) an eastward (away from the source) polarization of SV at COL; and (d) a northward polarization of SH at COL. The latter two correspond to positive radiation coefficients in the notation of Kanamori and Stewart [34]; furthermore, we have verified that the incidence angle at COL is small enough to keep the receiver function C^{SV} real positive ([35]; Fig. 4).

While both mechanisms I and IV support the dilatational first motion (a) at ABU, only I correctly predicts all three constraints (b–d), none of which would be compatible with IV. We thus select mechanism I ($\phi = 276°$; $\delta = 63°$; $\lambda = 70°$) as the final best double couple for the 1938 Banda Sea event.

This mechanism also correctly predicts the three dilatational (kataseismic) P-wave first motions reported by the ISS at Hong Kong, Zinsen (Incheon) and Heizyo (Pyongyang) and the compressional (anaseismic) one at Ksara, but contradicts the dilatational first motion reported at Bucharest. Note however that the latter two reports, obtained at neighboring stations on the focal sphere, are mutually incompatible, and thus incapable of resolving the focal mechanism. At any rate, first motions reported in bulletins from undocumented seismographs are notoriously unreliable, and are no match for polarities read individually on archived long-period instruments.

The location of the two aftershocks to the northeast of the main shock, possibly at a lesser depth, would favor the shallow-dipping plane ($\phi = 135°$; $\delta = 33°$; $\lambda = 124°$), but the poor depth control and the relatively large epicentral ellipses cannot preclude their occurrence on the steeply dipping plane; furthermore, they may not be true aftershocks, and could result from stress transfer on splay faults.

An intriguing report mentions the emergence, during the 1938 event, of a new island on the western side of the Kai group, at 5.72°S, 132.62°E, to an altitude of 5 m [25]. This location is shown as a star in Fig. 2. We computed tentative models of static surface displacement corresponding to both conjugate solutions for mechanism I, using Mansinha and Smylie's [36] algorithm and Geller's [37] global scaling laws to infer the geometry of rupture from the inverted value of M_0. Motion on the steep plane predicts a maximum vertical uplift of 2.4 m, but the Kai Islands are expected to undergo subsidence, while the shallow-dipping solution predicts only 1.8 m, with the Kai Islands generally nodal. Although it may be possible to adjust the position of the centroid and the distribution of slip on the fault to match the uplift at the reported location, we are concerned by the uniqueness of this report, i.e., by the absence of similar observations on the many

populated islands in the group, as well as by the relatively benign character of the tsunami observed in the Kai Islands, as compiled by Solov'ev and Go [38] who quote a maximum height of only 1 m. The emergence of the new island may be due to motion on a splay fault, or to a slow, post-seismic episode of relaxation.

Finally, we wish to comment on the only previously published mechanism (to the best of our knowledge) for the 1938 event, Ritsema and Veldkamp's [39] strike-slip solution ($\phi = 129°$; $\delta = 88°$; $\lambda = 162°$) as reported by Wickens and Hodgson [40]. This mechanism is clearly unacceptable as it grossly misfits the mantle wave radiation patterns and in particular the Rayleigh-to-Love ratios.

4. Discussion and conclusion

The principal results of this study are as follows.

4.1. The 1938 Banda Sea event is large

With $M_0 = 8.4 \times 10^{28}$ dyn-cm, our preferred solution makes it one of the 10 largest seismic moments ever computed [3]. Our results uphold the estimate by Brune and Engen [4] and Okal [5]. It is considerably larger than the largest CMT solutions found at comparable depths in the Harvard catalog, namely the 1994 Kuriles earthquake ($M_0 = 3 \times 10^{28}$ dyn-cm) and the 1977 Tonga earthquake ($M_0 = 1.8 \times 10^{28}$ dyn-cm), which Lundgren and Okal [41] have estimated to have ruptured from 40 to 125 km depth. The 1938 Banda Sea earthquake also dwarfs the 1963 shock ($M_0 = 3.1 \times 10^{28}$ dyn-cm [42]), located deeper and to the southwest, with which a detailed comparison is given below.

4.2. The 1938 Banda Sea event is relatively deep

Our centroid depth (60 km) is consistent with the rather minimal amount of damage wrought by the main shock. From the scant available reports [25], it appears that the earthquake was felt at no more than modified Mercalli intensity VI in the hardest hit areas (the Kai and Banda islands), and that it resulted in no casualties. Conversely, the event was felt strongly over a wide area, reaching Merauke and Darwin (Fig. 1). Finally, it generated a local tsunami, described as destroying beachfront property in Tajandu and Banda islands, but the only wave height reported is a mere 1 m [25,34], significantly less than observed in the regional field from modern events featuring smaller moments (e.g., Biak, 1996 [43]; Peru, 2001 [44]; Papua New Guinea, 2002 [45]). All of these observations clearly support a deeper than normal source for the 1938 earthquake.

The relocation of the epicenter near the Tajandu–Watubela arc as well as the depth of focus suggest that the earthquake took place either in the downgoing slab, or at the slab–mantle wedge interface. However, given the sparse seismicity in the immediate area, the precise mapping of the slab is uncertain.

4.3. The 1938 earthquake may involve the same component of compressional stress release as the 1963 event

Of the 21 recent shocks defined above as neighbors to the 1938 event, only four have published solutions in the Harvard catalog; it may be futile to compare these events to the 1938 earthquake, given the much smaller size of the former ($M_0 \leq 4.7 \times 10^{25}$ dyn-cm) and the large scatter in focal geometry among them (Fig. 3). Rather, it is more enlightening to compare the 1938 event with the large 1963 intermediate-depth earthquake 300 km to the southwest [42,46], shown as the open diamond in Fig. 2, whose mechanism is included in Fig. 3. We note in particular that the two P axes are sub-horizontal (plunging 16° at azimuth N21°E and 8° at azimuth N23°E, respectively) and are separated in space by only 8°. Thus, they probably express a coherent stress field due to the contortion of the subducting Australian lithosphere in the region [46]. This coherent direction of the compressional stress may also be representative of the azimuth of convergence (N19°E) between the Australian Plate and the supposedly undeformed Banda block, as computed at the Timor Trough using Rangin et al.'s

[26] model. As noted by Osada and Abe [42], this geometry is also reminiscent of the compressional stress released during the large 1964 South Sandwich intermediate-depth earthquake [47]. However, the 1938 Banda Sea earthquake is significantly shallower than the 1963 and 1964 earthquakes, whose hypocenters are given at 96 and 116 km, respectively, by Engdahl et al. [21].

4.4. The PDFM can work for large historical earthquakes

The final conclusion from this study is that the PDFM is a viable method for the robust, and hence reliable, moment tensor inversion of large historical earthquakes for which a handful of long-period seismograms, with little or no precise timing, are available. While the modeling of datasets consisting exclusively of spectral amplitudes in order to retrieve the focal geometry of large earthquakes was pioneered more than 30 years ago principally by Kanamori [48,49], this approach remained largely a process of trial and error. In this respect, the advantage of the PDFM concept is that of an inversion technique, ensuring that the solution obtained in the parameter space will indeed correspond to a formal optimization of the dataset of observables. Our case study of the 1938 Banda Sea sets the stage for the more systematic use of the method to unravel the mechanism of large historical earthquakes.

Acknowledgements

We are grateful to Ota Kulhánek, Don Helmberger, Jim Dewey and John Ebel, for welcoming us to their observatories and helping with the retrieval of precious historical seismograms from their archives. We thank Hiroo Kanamori for discussion on the response of the early Benioff prototypes at Pasadena, Bob Engdahl for an update of his catalog [21] and a customized relocation of the 1938 main shock, and Giovanni Sella for a perspective on GPS results in the region. Constructive comments by Rachel Abercrombie, Antonio Villaseñor and two anonymous reviewers improved the original manuscript.*[SK]*

References

[1] D. Reymond, E.A. Okal, Preliminary determination of focal mechanisms from the inversion of spectral amplitudes of mantle waves, Phys. Earth Planet. Inter. 121 (2000) 249–271.
[2] B. Gutenberg, C.F. Richter, Seismicity of the Earth and Associated Phenomena, Princeton University Press, Princeton, NJ, 1954, 310 pp.
[3] H. Kanamori, The energy release in great earthquakes, J. Geophys. Res. 82 (1977) 2981–2987.
[4] J.N. Brune, G.R. Engen, Excitation of mantle Love waves and definition of mantle wave magnitude, Bull. Seismol. Soc. Am. 59 (1969) 923–933.
[5] E.A. Okal, Use of the mantle magnitude M_m for the reassessment of the seismic moment of historical earthquakes. I: Shallow events, Pure Appl. Geophys. 139 (1992) 17–57.
[6] B.A. Romanowicz, G. Suárez, On an improved method to obtain the moment tensor and depth of earthquakes from the amplitude spectrum of Rayleigh waves, Bull. Seismol. Soc. Am. 73 (1983) 1513–1526.
[7] H. Patton, K. Aki, Bias in the estimate of seismic moment tensor by the linear inversion method, Geophys. J. R. Astron. Soc. 59 (1979) 479–495.
[8] W.-C. Huang, E.A. Okal, G. Ekström, M.P. Salganik, Centroid moment tensor solutions for deep earthquakes predating the digital era: The historical dataset (1907–1961), Phys. Earth Planet. Inter. 106 (1998) 181–190.
[9] W.B. Hamilton, Tectonics of the Indonesian region, U.S. Geol. Surv. Prof. Pap. 1078 (1979) 345 pp.
[10] N. Chamot-Rooke, X. Le Pichon, GPS determined eastward Sundaland motion with respect to Eurasia confirmed by earthquake slip vectors at Sunda and Philippine trenches, Earth Planet. Sci. Lett. 173 (1999) 439–455.
[11] G.W. Michel, M. Becker, D. Angermann, C. Reigber, E. Reinhart, Crustal motion in E- and SE-Asia from GPS measurements, Earth Planets Space 52 (2000) 713–720.
[12] M. Untung, Subsidence of the Aru Trough and the Aru Island, Irian Jaya, Indonesia, Tectonophysics 112 (1985) 411–422.
[13] T.R. Charlton, S.J. Kaye, H. Samodra, Geology of the Kai Islands: implications for the evolution of the Aru Trough and Weber Basin, Banda Arc, Indonesia, Mar. Petrol. Geol. 8 (1991) 62–69.
[14] J. Milsom, S. Kaye, Extension, collision and curvature in the Eastern Banda Arc, Geol. Soc. London Spec. Publ. 106 (1996) 85–94.
[15] R. McCaffrey, Active tectonics of the Eastern Sunda and Banda Arcs, J. Geophys. Res. 93 (1988) 5163–15182.
[16] A.R. Ritsema, New seismicity maps of the Banda Sea, J. Sci. Res. Indon. 2 (1953) 48–54.
[17] R.K. Cardwell, B.L. Isacks, Geometry of the subducted lithosphere beneath the Banda Sea in Eastern Indonesia from seismicity and fault plane solutions, J. Geophys. Res. 83 (1978) 2825–2838.
[18] R. McCaffrey, P. Molnar, S. Roecker, Y. Joyodiwiryo,

Microearthquake seismicity and fault plane solutions related to arc-continent collision in the Eastern Sunda Arc, Indonesia, J. Geophys. Res. 90 (1985) 4511–4528.
[19] R. McCaffrey, Slip partitioning at convergent plate boundaries of SE Asia, Geol. Soc. London Spec. Publ. 106 (1996) 3–18.
[20] J. Milsom, Subduction in eastern Indonesia: how many slabs?, Tectonophysics 338 (2001) 167–178.
[21] E.R. Engdahl, R.D. van der Hilst, R.P. Buland, Global teleseismic earthquake relocation with improved travel times and procedures for depth determination, Bull. Seismol. Soc. Am. 88 (1998) 722–743.
[22] A.M. Dziewonski, G. Ekström, J.E. Franzen, J.H. Woodhouse, Global seismicity of 1977; Centroid moment tensor solutions for 471 earthquakes, Phys. Earth Planet. Inter. 45 (1987) 11–36.
[23] C. Honthaas, R.C. Maury, B. Priadi, H. Bellon, J. Cotten, The Plio-Quaternary Ambon Arc, Eastern Indonesia, Tectonophysics 301 (1999) 261–281.
[24] M.E. Wysession, E.A. Okal, K.L. Miller, Intraplate seismicity of the Pacific Basin, 1913–1988, Pure Appl. Geophys. 135 (1991) 261–359.
[25] Anonymous, Aardbevingen in den Oost Indischen Archipel waargenomen gedurende het jaar 1938, Natuurk. Tijdschr. Ned. Indie 40 (1940) 38–74.
[26] C. Rangin, X. Le Pichon, S. Mazzotti, M. Pubellier, N. Chamot-Rooke, M. Aurelio, A. Walpersdof, R. Quebral, Plate convergence measured by GPS across the Sundaland/Philippine Sea Plate deformed boundary: the Philippines and Eastern Indonesia, Geophys. J. Int. 139 (1999) 296–316.
[27] H.E. McComb, C.J. West, List of seismological stations of the world, Bull. Natl. Res. Council 82 (1931) 118 pp.
[28] C. Charlier, J.-M. van Gils, Liste des stations séismologiques mondiales, Obs. R. Belg. Uccle, 1953, 282 pp.
[29] D. Reymond, O. Hyvernaud, J. Talandier, Automatic detection, location and quantification of earthquakes: application to tsunami warning, Pure Appl. Geophys. 135 (1991) 361–382.
[30] E.A. Okal, J. Talandier, M_m: A variable period mantle magnitude, J. Geophys. Res. 94 (1989) 4169–4193.
[31] E.A. Okal, J. Talandier, M_m: Extension to Love waves of the concept of a variable-period mantle magnitude, Pure Appl. Geophys. 134 (1990) 355–384.
[32] J.B. Minster, T.H. Jordan, P. Molnar, E. Haines, Numerical modelling of instantaneous plate tectonics, Geophys. J. R. Astron. Soc. 36 (1974) 541–576.
[33] Y.Y. Kagan, 3-D rotation of double-couple earthquake sources, Geophys. J. Int. 106 (1991) 709–716.
[34] H. Kanamori, G.S. Stewart, Mode of the strain release along the Gibbs fracture zone, Mid-Atlantic Ridge, Phys. Earth Planet. Inter. 11 (1976) 312–332.
[35] E.A. Okal, A student's guide to teleseismic body-wave amplitudes, Seismol. Res. Lett. 63 (1992) 169–180.
[36] L. Mansinha, D.E. Smylie, The displacement fields of inclined faults, Bull. Seismol. Soc. Am. 61 (1971) 1433–1440.
[37] R.J. Geller, Scaling relations for earthquake source parameters and magnitudes, Bull. Seismol. Soc. Am. 66 (1976) 1501–1523.
[38] S.L. Solov'ev, Ch.N. Go, Catalogue of tsunamis on the western shore of the Pacific Ocean, Can. Transl. Fish. Aquat. Sci. 5077 (1984) 439 pp.
[39] A.R. Ritsema, J. Veldkamp, Fault plane mechanisms of southeast Asian earthquakes, Publ. Konink. Ned. Meteor. Inst. 72 (1960) 63 pp.
[40] A.J. Wickens, J.H. Hodgson, Computer re-evaluation of earthquake mechanism solutions, Publ. Dominion Observ. 33 (1967) 560 pp., Ottawa, ON.
[41] P.R. Lundgren, E.A. Okal, Slab decoupling in the Tonga arc: the June 22, 1977 earthquake, J. Geophys. Res. 93 (1988) 13355–13366.
[42] M. Osada, K. Abe, Mechanism and tectonic implications of the great Banda Sea earthquake of November 4, 1963, Phys. Earth Planet. Inter. 25 (1981) 129–139.
[43] H. Matsutomi, N. Shuto, F. Imamura, T. Takahashi, Field survey of the 1996 Irian Jaya earthquake tsunami in Biak Island, Nat. Hazards 24 (2001) 199–212.
[44] E.A. Okal, L. Dengler, S. Araya, J.C. Borrero, B. Gomer, S. Koshimura, G. Laos, D. Olcese, M. Ortiz, M. Swensson, V.V. Titov, F. Vegas, A field survey of the Camaná, Perú tsunami of June 23, 2001, Seismol. Res. Lett. 73 (2002) 904–917.
[45] J.C. Borrero, J. Bu, C. Saiang, B. Uslu, J. Freckman, B. Gomer, E.A. Okal, C.E. Synolakis, Field survey and preliminary modeling of the Wewak, Papua New Guinea earthquake and tsunami of September 9, 2002, Seismol. Res. Lett. 74 (2003) 393–405.
[46] J.L. Welc, T. Lay, The source rupture of the great Banda Sea earthquake of November 4, 1963, Phys. Earth Plan. Inter. 45 (1987) 242–254.
[47] K. Abe, Focal process of the South Sandwich Islands earthquake of May 26, 1964, Phys. Earth Planet. Inter. 5 (1972) 110–122.
[48] H. Kanamori, Synthesis of long-period surface waves and its application to earthquake source studies – Kurile Islands earthquake of October 13, 1963, J. Geophys. Res. 75 (1970) 5011–5027.
[49] H. Kanamori, The Alaska earthquake of 1964: Radiation of long-period surface waves and source mechanism, J. Geophys. Res. 75 (1970) 5029–5040.